THE JOURNAL OF PHYSICAL CHEMISTRY Letters

Perspective

pubs.acs.org/JPCL

Molecular Insights into Carbon Supercapacitors Based on Room-Temperature Ionic Liquids

Guang Feng,[†] Song Li,[†] Volker Presser,[‡] and Peter T. Cummings*[,†,§]

[†]Department of Chemical and Biomolecular Engineering, Vanderbilt University, Nashville, Tennessee 37235, United States

[‡]INM – Leibniz Institute for New Materials, Energy Materials Group & Saarland University, Campus D2 2, 66123 Saarbrücken, Germany

[§]Center for Nanophase Materials Sciences, Oak Ridge National Laboratory, Oak Ridge, Tennessee 37831, United States

ABSTRACT: The performance of supercapacitors is determined by the electrical double layers (EDLs) formed at electrolyte/electrode interfaces. To understand the energy storage mechanism underlying supercapacitors, molecular dynamics (MD) simulations were used to study the capacitive behavior of carbon-based supercapacitors with room-temperature ionic liquid (RTIL) electrolytes. The performance of porous supercapacitors was found to be correlated with the ion/pore size and applied voltage. Supercapacitors composed of RTILs on the outer, positively curved surfaces of onion-like carbons (OLCs) or carbon nanotubes (CNTs) exhibited significant effects on capacitance and the distinctive feature that differential capacitance varies only weakly with voltage. Investigations of temperature influence revealed a positive temperature dependence of capacitance for OLC-based supercapacitors and a weak dependence of capacitance on temperature for CNT-based supercapacitors, in line with experimental observations. Molecular insights into RTIL-based supercapacitors, reviewed in this Perspective, could facilitate the design and development of a new generation of energy storage devices.

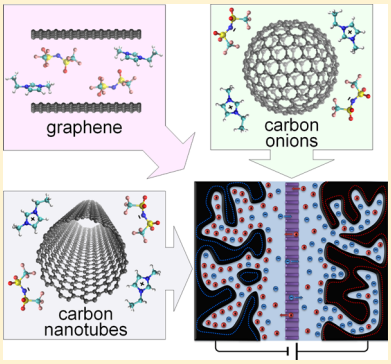

The use of electricity generated from renewable but intermittent energy sources (e.g., solar and wind) requires concepts for efficient energy storage.[1,2] Electrical energy storage (EES) devices are a rising star on the horizon of energy storage technologies, and among them, electrical double-layer capacitors (EDLCs), also called ultracapacitors or supercapacitors, have received a great deal of attention in recent years due to their advantageous properties, such as high power density, high capacitance, and excellent performance stability.[3−5] Supercapacitors store electrical energy via ion electrosorption directly in the EDLs at the electrolyte/electrode interface, and the EDL plays a dominant role in the underlying energy storage mechanism and the resulting device performance. Pseudocapacitors, that is, EES systems that combine capacitive and redox charge storage, are under intense active investigation but are not part of this Perspective.[6,7] With a moderate energy density compared to batteries, the essence of current supercapacitor development is to optimize their charge storage capacity by enlarging the electrode surface area and/or increasing the maximum cell voltage. Both parameters, the capacitance and the cell voltage, limit the amount of energy that can be stored and have stimulated tremendous research activities both in the material science of the electrodes and organic chemistry of the electrolytes. Thus, choosing an appropriate combination of electrolytes and electrode materials is essential. Because of their exceptionally wide electrochemical window, excellent thermal stability, nonvolatility, and relatively inert nature, room-temperature ionic liquids (RTILs) have become emerging candidates for electrolytes used in supercapacitors.[8−11] With the high specific surface area (SSA), good electrical conductivity, chemical stability in a variety of electrolytes, and relatively low cost, presently carbons are the most widely used electrode materials in supercapacitors.[4,12−14] To improve the energy density and the transport properties of the charge carriers in supercapacitors, carbons have been developed in diverse forms such as activated carbons,[15] carbide-derived carbons (CDCs),[16] carbon nanotubes (CNTs),[17,18] onion-like carbons (OLCs),[19,20] graphene,[21,22] and so on. On the basis of the pore geometry of carbon electrodes and the way that electrolyte ions interact with the electrode surface, in this Perspective, from the view of modeling, supercapacitors are classified into three categories:[23−25] (i) the term "endohedral supercapacitor" is used to denote supercapacitors with porous carbon electrodes showing a zero or negative surface-curved pore where ions can enter inside (i.e., the charge stored in the pore, e.g., ions inside open-ended CNTs), (ii) the term "exohedral supercapacitor" is for supercapactiors in which ions reside on the outer surface of carbon particles (i.e., the charge stored on the positively curved surfaces, e.g., ions on outside surfaces of OLCs and end-capped CNTs), and (iii) the term "planar supercapacitor" is for supercapacitors with zero/negligible curvature of the electrode (e.g., flat graphene sheets). Note that, "endohedral", "exohedral", and "planar" are adopted here for the description of different electrode surfaces that

Received: July 9, 2013
Accepted: September 12, 2013

   dx.doi.org/10.1021/jz4014163 | J. Phys. Chem. Lett. 2013, 4, 3367−3376

electrolyte ions adsorb on rather than the shape of supercapacitors; although a real supercapacitor may contain endohedral, exohedral, and planar electrode surfaces, one type of the electrode surface is usually modeled in a simulation to study a specific or dominate phenomenon in a supercapacitor.

> Accurate control of the pore size distribution of porous electrodes is crucial for the design of high-performance supercapacitors.

Common endohedral supercapacitor electrode materials are porous carbons such as activated carbons, templated carbons, and CDCs, which can show a high or very high SSA and a high energy density.[4,13,26−28] By reducing the pore size of microporous carbon, experiments on CDCs[27] and activated carbon[28] in an organic electrolyte of tetraethylammonium tetrafluoroborate ([TEA][BF_4]) in the aprotic solvent acetonitrile (ACN) revealed an increase of the capacitance (normalized by either the surface area or pore volume) at pore sizes less than 1 nm. Similar trends have been reported experimentally for carbon supercapacitors with aqueous electrolytes (e.g., KOH solution).[28,29] Using the RTIL 1-ethyl-3-methylimidazolium bis(trifluoromethylsulfonyl)imide ([emim][Tf_2N]) as the electrolyte, Largeot et al.[30] observed a dramatic increase of capacitance within the pore sizes of 0.65−1.1 nm, and the capacitance was maximized at a pore size of 0.7 nm comparable to the ion size. To rationalize the capacitance increase in micropores, phenomenological models were proposed, including the electric wire-in-cylinder capacitor model[24] for cylindrical pores and the sandwich model[31] for slit-shaped pores, which provided a good fit to experimental data. On the basis of mean-field theory and Monte Carlo (MC) simulations, Kondrat et al.[32,33] attributed the increase of capacitance to the "superionic state" of ions inside pores. Taking into account the van der Waals interactions and complex ionic structure, molecular dynamics (MD) simulations have reproduced the capacitance−voltage trend measured in experiments with both solvent electrolytes and RTILs.[34,35]

The capacitance increase at small pore sizes, observed in aqueous, organic, and IL electrolytes experimentally and reproduced in simulation, is a universal phenomenon for supercapacitors based on microporous carbons. However, a recent experimental study by Centeno et al. reported a regular (i.e., pore-size-independent) normalized capacitance of carbon pores with a size of 0.7−15 nm, using the same electrolyte of [TEA][BF_4]/ACN.[36] This challenging experimental observation raised issues concerning the existence of the enhancement of micropore capacitance and how the capacitance changes over a wide range of pore size, including the "anomalous increase" regime. To address these issues, we performed MD simulations of EDLs inside micropores with RTIL [emim][Tf_2N] and employed theoretical studies on the ions inside carbon pores, serving as in-depth information on the atomistic scale inherent in the experiment.[37]

As shown in Figure 1, over a broad range of pore sizes (i.e., the slit width, d) from 0.67 to 1.8 nm, the capacitance of slit-shaped micropores under the applied potential of ∼1.4 V was found to oscillate with pore size, decreasing toward C_∞ (=0.068 F/m^2), the capacitance of EDL near-planar carbon electrodes with the open surface.[37] Specifically, in the first peak of the $C-d$ (capacitance versus pore size) curve, the capacitance increase

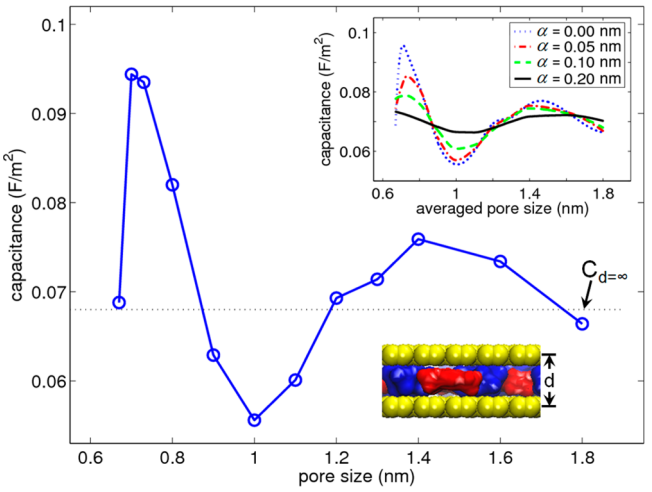

Figure 1. Specific capacitance of the micropore as a function of pore size. The blue line connecting the circular symbols represents MD simulation results. C_∞ (=0.068 F/m^2) is the capacitance of EDL near-planar carbon electrodes with the open surface. The lower inset shows the snapshot of the slit-shaped pore (yellow-colored walls) filled with RTILs (red-colored cations and blue-colored anions), where d is the slit-shaped pore size; the upper inset exhibits the curves of capacitance versus pore size at varying pore size distributions, under an assumption that the pore size distribution follows different Gaussian functions, where α is its standard deviation that describes the broadness of the pore size distribution.

does exist as the pore size reduces from 1.0 to 0.7 nm, fully consistent with experimental observations by Gogotsi and coworkers;[27,30,38] the capacitance reaches a maximum at the pore size of 0.7 nm, which is similar to the ion size, and then goes down as the pore size continues decreasing, consistent with experimental findings of porous carbon supercapacitors with the same electrolyte.[12,22] Another feature is the second peak of the $C-d$ curve occurring within 1.0−1.8 nm, and the maximum is located at 1.4 nm; this feature, only observed when modeling a very narrow (i.e., monodisperse) pore size distribution, has not yet been reported experimentally. The U-shaped scaling behavior between two maxima was observed concurrently in other MD work,[39] in which electrode surface polarizability was taken into account and a united atom coarse-grain model was used for an imidazolium-based RTIL. Concurrently, a density functional theory (DFT) study,[40] in which the electrolyte ions were represented by charged hard spheres and the van der Waals interactions and complex ionic structure were neglected, not only reproduced the capacitance increase under nanopores but also predicted more than two peaks in the $C-d$ curve, suggesting that the oscillatory behavior of capacitance could be a generic feature of porous supercapacitors with RTIL electrolytes. It is worthwhile to note that this oscillatory behavior of capacitance over a broad pore size does not hold for electrolytes in organic solvent.[41]

The oscillatory $C-d$ curve predicted in simulation, including the capacitance increase for micropores, seems to conflict with capacitance independent of the pore size reported experimentally by Centeno et al.[36] However, it is noted that the pore size in simulation is a single value (i.e., perfectly monodisperse), while the pore size in experiment is an averaged value over a range of pore sizes. For the inset in Figure 1, the pore size distribution is assumed to follow a Gaussian function, $f(x) = (1/(\alpha(2\pi)^{1/2}))\exp[-(x/\alpha)^2/2]$, where α is its standard

dx.doi.org/10.1021/jz4014163 | J. Phys. Chem. Lett. 2013, 4, 3367−3376

deviation that describes the broadness of the pore size distribution. Using the simulation results, under the assumption that different sized pores are independent, the $C-d$ curves for different pore size distributions were recomputed as a function of averaged pore size. This calculation shows that the capacitance oscillation becomes less well-defined with broadening pore size distribution. For instance, as α = 0.1 nm, the capacitance in the micropore varies from −10.5 to 15.8%, which is quite close to that of ±11.7% in the experiment by Centeno et al. reporting the absence of the increased capacitance.[36] This suggests that the increase as well as the oscillation of capacitance could be washed out in experiments based on a carbon material exhibiting a broad pore size distribution. Therefore, accurate control of the pore size distribution of porous electrodes is crucial for the design of high-performance supercapacitors. However, the regular pattern of capacitance versus pore size could alternatively be attributed to the 20 wt % binder plus 5 wt % of carbon black additive in the electrode (as described in Experimental Section of ref 36). This could also result in smearing the dependence of the capacitance on the pore size.

Theoretically, using the quantitative model described by eq 1 and knowing the structure and capacitance of the EDL at the planar electrode with open surface, one can predict how the capacitance varies with pore size.

To understand the physical origin of the oscillatory behavior of the $C-d$ curve in Figure 1, we introduced a concept of EDL interference, as illustrated in Figure 2. Similar to the wave interference, the EDL in a slit pore can be considered as a result of interference between two EDLs stemming from two opposite-facing slit walls. These two EDLs shown in Figure 2a are described by their number density profiles of $\rho_n(z)$ and $\rho_n(d - z)$ near the open surface of the planar electrode, respectively.[37] By superposing the number density profile from each slit wall, the resultant EDL structure inside a slit pore through the EDL interference is obtained as $\rho_n^S(z) = \rho_n(z) + \rho_n(d - z)$. As shown in Figure 2b, the superposition-predicted EDL structure by the EDL interference in a 1.4 nm wide slit is similar to that directly computed in MD simulation. The interference effect on EDLs inside a slit pore is quantified by the effective EDL interference factor, defined as[37]

$$f_{EI}(d) = \left(\frac{W_{EDL} + d}{d}\right)\frac{\int_0^d \rho_n^O(z)\,dz}{2\int_0^d \rho_n^S(z)\,dz} \quad (1)$$

where $\rho_n^O(z) = \min[\rho_n(z), \rho_n(d - z)]$ represents the overlapping part of two EDLs by their interference (Figure 2b) and W_{EDL} is the thickness of the EDL observed in MD simulation. The effective interference factor (f_{EI}) was calculated and shown as a function of pore size in Figure 3 using an EDL

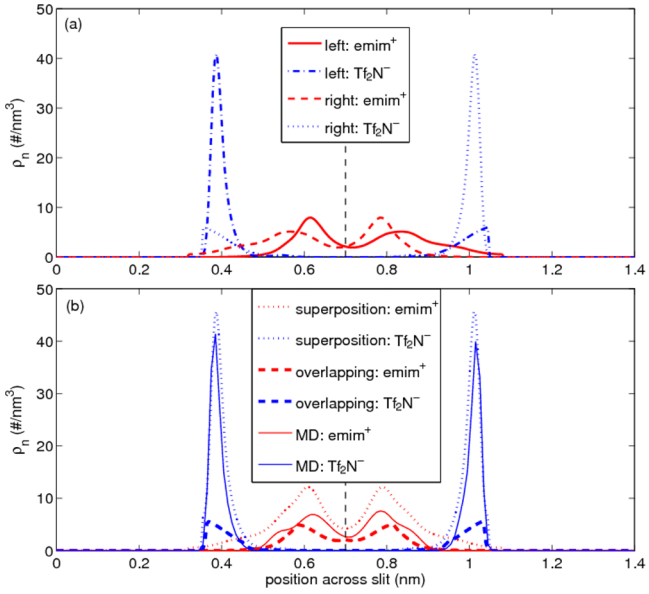

Figure 2. Interference of EDL structure: (a) ion number density profiles from two opposite-facing (left and right) slit walls; (b) superposition and overlapping of ion number densities in a slit with a size of 1.4 nm. The vertical black dashed line in each panel represents the central position at which the EDLs are symmetrized. Adapted from ref 37. Copyright 2011, American Chemical Society.

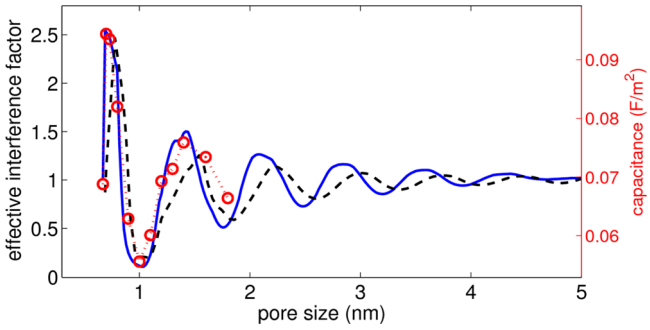

Figure 3. Effective interference factor as a function of pore size. The solid blue line (left axis) represents the effective interference factor for RTIL [emim][Tf_2N]; the black dashed line (left axis) is for RTIL [bmim][Tf_2N]; the dotted line with red circular symbols (right axis) is the $C-d$ curve shown in Figure 1.

at the open surface under the applied potential of ∼1.4 V. We can observe that within 0.67−1.8 nm, the effective interference factor has the same trend as the overall $C-d$ curve. On the basis of eq 1, the larger f_{EI} indicates that more ions could pack into the slit due to the constructive interference, evidenced by the intensity of ion peaks in Figure 2a, which results in an enhancement of the capacitance of micropores; destructive interference can reduce the capacitance by lessening the ion packing inside micropores. Beyond the two-peaked $C-d$ curve obtained by MD simulation, the effective interference factor still exhibits an oscillatory behavior but becomes weaker with decaying amplitude, approaching to unit at ∼4.5 nm, which is similar to that predicted in a DFT study.[40] The distance between two peaks is about 0.7 nm, compatible with the RTIL ion size. Theoretically, using the quantitative model described by eq 1 and knowing the structure and capacitance of the EDL at the planar electrode with open surface, one can predict how the capacitance varies with pore size. The effective interference factor for supercapacitors with the RTIL 1-butyl-3-methylimidazolium bis(trifluoromethylsulfonyl)imide [bmim][Tf_2N] was also computed in Figure 3, which implies that the capacitance of carbon pores filled with [bmim][Tf_2N] also

dx.doi.org/10.1021/jz4014163 | J. Phys. Chem. Lett. 2013, 4, 3367−3376

exhibits oscillatory behavior but with a larger gap between peaks. Note that this predictive model based on the EDL interference was developed initially for a slit-shaped pore and may require further confirmation/modification for different-shaped pores (e.g., cylindrical pores have negative curvature).

The influence of the electrode potential on capacitance has been investigated to understand the charging mechanism of porous carbon supercapacitors. Using MC simulations, Kondrat et al.[33,43] revealed that for different-sized slit pores, the differential capacitance changes slightly at low voltage, mostly increases to a maximum, and then decays to zero due to the saturation of the total charge accumulated in a pore at moderate/large voltages. In particular, the voltage where the maximum of differential capacitance occurs depends on the pore size, which suggests that the oscillatory $C-d$ curve may also differ under different applied voltages. Later, by modeling a 0.78 nm wide slit-shaped pore filled with RTIL [dmim][BF_4] in MD simulation, Wu et al.[42] reported a similar voltage-dependent capacitance, as shown in Figure 4; note, however,

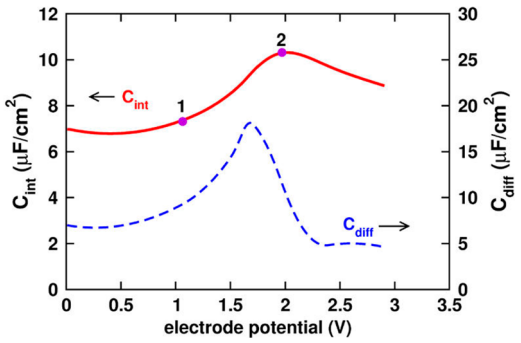

Figure 4. The integral capacitance (C_{int}) and differential capacitance (C_{diff}) of a 0.78 nm wide slit-shaped pore as a function of electrode voltage. The state points 1 and 2 represent the capacitances at the electrode voltages of 1.07 and 1.97 V, respectively. Adapted from ref 42. Copyright 2012, American Chemical Society.

that unlike the simulations results of Kondrat et al.,[33,43] the MD calculations do not exhibit ion saturation under large potentials (~3 V). The charge storage in subnanometer pores exhibits rich behaviors as the voltage increases; the capacitance (both integral and differential) changes weakly at voltages less than 1 V, which is explained by co-ions inside the pore swapping with counterions outside the pore so that the net charge of the pore interior varies nearly linearly with potential; as the potential keeps increasing, the capacitance increases as well and reaches a maximum at a particular voltage. This behavior is mainly attributed to the removal of co-ions from the pore; beyond the maximum point, the capacitance increase is primarily dominated by the counterion insertion into the pore.[42]

Assuming similar capacitance change under both negative and positive voltages in Figure 4, the overall capacitance–voltage relation would exhibit a camel-like shape, which was observed by Xing et al.[44] using a combined explicit and united atom model for RTILs. Furthermore, the bell- and U-shaped capacitance–voltage relations were observed for different-sized pores in the same work.[44] A DFT study also showed a bell-shaped curve due to the co-ion removal of and counterion addition.[45] The absence of capacitance increase observed in DFT calculations is probably due to the simplified RTIL ions in the restricted primitive model and the selected pore size. Hence, the voltage-dependent capacitance may depend on the specific nature of both the RTILs and the pores.

Recently, exohedral supercapacitors with electrodes consisting of OLCs or CNTs have been developed to enhance the device power handling due to the readily accessible electrode surface; in contrast, endohedral supercapacitors with narrow micropores may slow down the charge/discharge rate because of limited ion mobility.[46] For example, the discharge rates of OLC-based supercapacitors (namely, 200 V/s) were measured to be 3 orders of magnitude higher than those of conventional supercapacitors;[19] densely packed and aligned single-walled carbon nanotubes (SWCNTs) have been shown to be excellent electrodes, allowing supercapacitors to achieve higher power density (>40 kW/kg),[47,48] especially when SWCNTs were aligned parallel to the direction of electrolyte ion transport.[49] To rationalize the relation of capacitance and the size of the OLC or CNT, Huang et al.[25] proposed two phenomenological models, the exohedral electric double-sphere capacitor (xEDSC) model for spherical electrodes and the exohedral electric double-cylinder capacitor (xEDCC) model for cylindrical electrodes. Although both theoretical models show that the EDL capacitance increases as the size of spherical/cylindrical electrodes decreases, the origin of such curvature effects has not yet been fully understood. The most extensively studied macroscopic property of the EDLs in RTILs is the differential capacitance versus the applied potential (i.e., the $C-V$ curve).[50,51] Many efforts have been made to demonstrate that there are different $C-V$ curves observed and predicted for planar supercapacitors (e.g., the U-shaped, bell-shaped, and camel-shaped ones).[50−55] However, few studies have focused on how the differential capacitance changes with applied potentials for exohedral supercapacitors with OLC/CNT-based electrodes and RTIL electrolytes.

The weak potential dependence of the capacitance of the EDL near nanosized OLC and CNT electrodes provides an attractive design tool for supercapacitors with improved performance.

We performed MD simulations of OLCs and end-capped CNTs immersed in the RTIL [emim][Tf_2N] to investigate the effects of electrode size and potential on the capacitance of exohedral supercapacitors. Note that in the work reported herein, for OLCs/CNTs-based supercapacitors, the image charge effect stemming from the electrode is neglected, and the partial charges are placed on the carbon atoms of the electrode rather than on an image plane, which differs from our previous work in ref 56. The differential capacitance as a function of voltage is shown in Figure 5 for exohedral supercapacitors based on OLCs and CNTs and for planar supercapacitors with flat graphene sheets as electrodes. It can be seen that there is a bell-shaped $C-V$ curve for EDLs in RTILs near the planar electrode, in line with previous studies;[57] for the exohedral supercapacitors based on OLCs/CNTs, the differential capacitance depends weakly on the electrode voltage, which differs from the U-, bell-, or camel-shaped $C-V$ curves observed on planar electrodes.[50−55] This feature becomes more pronounced with reducing size of the OLC or CNT. The capacitance of EDL near the OLC-based electrode is

dx.doi.org/10.1021/jz4014163 | J. Phys. Chem. Lett. 2013, 4, 3367−3376

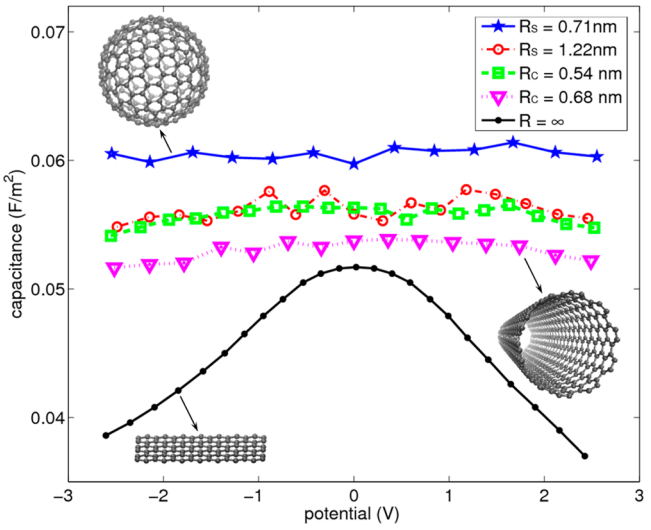

Figure 5. Influence of electrode curvature on the differential capacitance. R_S is the radius of the spherical OLC electrode, R_C is the radius of the cylindrical CNT electrode, and R is infinity for the planar graphene electrode.

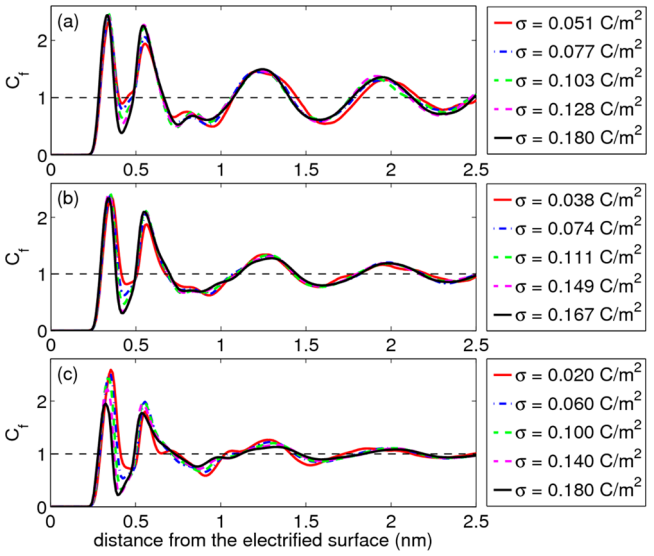

Figure 6. The charge screening factor (C_f) across EDLs in the RTIL [emim][Tf_2N] near (a) spherical electrodes (radius of 0.71 nm), (b) cylindrical electrodes (radius of 0.68 nm), and (c) planar electrodes with different surface charge densities.

larger than that of identical-sized CNTs, and the capacitances for both OLC- and CNT-based electrodes are higher than that near planar graphene. The weak potential dependence of the capacitance of the EDL near nanosized OLC and CNT electrodes invites further experimental exploration to take advantage of this phenomenon and could benefit the future design and improvement of supercapacitors with stable performance by fabricating electrodes with spherical and/or cylindrical nanoscale-curved surfaces.

The voltage-dependent differential capacitance of EDLs near the planar electrode can be explained by charge overscreening at small/moderate voltages and the lattice saturation evolved at large voltages.[57,58] In this context, the charge overscreening describes the phenomenon that the counter-charge from the first ion layer adsorbed on the electrode exceeds that on the electrode surface, and lattice saturation indicates that near highly charged surfaces, more than one consecutive layer of counterions can accumulate on the electrode.[50,57−59] Many studies have revealed that because of the high ionic density and strong ion coupling in RTILs, charge overscreening is a universal feature of EDLs at the interfaces of RTILs and electrodes.[50,57−61] To quantify the charge screening along the EDL, a charge-screening factor was introduced as follows[62]

$$C_f(u) = -\frac{1}{\sigma}\int_{u_0}^{u}\left(\frac{s}{R}\right)^N \Delta\rho_e(s)\,\mathrm{d}s \qquad (2)$$

where u_0 represents the location of the electrode surface: $u_0 = 0$ is for the planar electrode, and $u_0 = R$ is the size of OLC/CNT; N = 0, 1, and 2 are for planar, cylindrical, and spherical electrodes, respectively; $\Delta\rho_e$ is the variation of space charge density across EDLs as the surface charge density increases from 0 to σ. For C_f greater than unity, charge overscreening occurs, and the height of the first peak in C_f is used to quantify the degree of charge overscreening of the EDL. Figure 6 shows the charge screening factors across EDLs in the RTIL [emim][Tf_2N] near spherical, cylindrical, and planar carbon electrodes. It can be seen that as the electrode becomes more charged, the planar electrode is less overcharged; whereas the charge overscreening varies little for both OLC and CNT electrodes. This leads to the observed trend of $C-V$ curves near different electrodes. That is, within the working voltage range studied here, the bell shaped $C-V$ curve arises because planar electrodes in RTILs experience a potential-dependent decay in the charge overscreening; the near-flat $C-V$ curves originate from the fact that nanocurved spherical and cylindrical electrodes achieve nearly constant charge overscreening that is weakly dependent on the applied potential.[56,62] Note that charge overscreening only qualitatively probes the capacitance−potential relationship. Further explorations are needed to establish a quantitative model between charge overscreening and the capacitance, including the electrode curvature and ion size.

The curvature of the OLC/CNT-based electrode not only has a significant impact on the trend of $C-V$ curves (Figure 5) but also plays an important role in the capacitance magnitude. Figure 7a shows the relation between spherical and cylindrical curvatures originating from OLCs and CNTs and the integral capacitance under an applied potential of ∼1.4 V for a one-

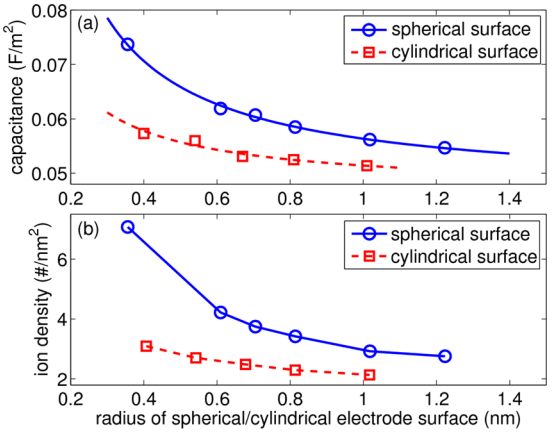

Figure 7. (a) Relation between the integral EDL capacitance and OLC/CNT radius. (b) Accumulative ability of counterions near OLCs/CNTs under a potential of ∼1.4 V.

dx.doi.org/10.1021/jz4014163 | J. Phys. Chem. Lett. 2013, 4, 3367−3376

electrode setup. It is observed that the capacitance of EDLs near spherical/cylindrical surfaces increases with electrode curvature or as the radius of spherical/cylindrical surfaced electrodes decreases; the capacitance for a spherical surface is larger and increases faster than that of a cylindrical surface. The capacitance−radius relation for the exohedral supercapacitor was studied by Huang et al.[25] with the xEDSC model for spherical electrodes in a scaling equation of the form

$$C = \varepsilon_r \varepsilon_0 \left(\frac{1}{R} + \frac{1}{d_{EDL}} \right) \tag{3}$$

and the xEDCC model for cylindrical electrodes as

$$C = \frac{\varepsilon_r \varepsilon_0}{R \ln(1 + d_{EDL}/R)} \tag{4}$$

where ε_0 is the vacuum permittivity, ε_r is the dielectric constant of the EDL, and d_{EDL} is the effective thickness of an EDL. Fitting simulation results (Figure 7a) to the above two phenomenological models gives ε_r = 1.12 and d_{EDL} = 0.22 nm for EDLs near the spherical-surfaced electrode and ε_r = 1.47 and d_{EDL} = 0.29 nm for cylindrical-surfaced electrode. Although the fitting parameters of ε_r and d_{EDL} are reasonable physically (e.g., the dielectric constant is larger than the vacuum value of 1 and smaller than that of bulk [emim][Tf_2N], and the effective EDL thickness is compatible with the ion size), we have to point out that ε_r and d_{EDL} are fitting values obtained *implicitly* by the phenomenological models expressed in the form of eqs 3 and 4 rather than the physical measurements obtained *explicitly* from simulation or experiment. The increased ion accumulation on the electrode was found to be responsible for the EDL capacitance enhancement due to the electrode curvature.[56,62] That is, under an applied potential, as the electrode curvature increases, more ions per surface area can be packed. The accumulative ability of ion packing was quantified by the ion number density normalized by the electrode surface area. As shown in Figure 7b, per unit surface area, more ions can be accumulated on the more curved electrode, and a spherical-surfaced electrode exhibits stronger ion accumulative ability than the cylindrical one because the spherical surface is zero-dimensional and the cylindrical surface is one-dimensional and the spherical surface can provide more space for ion adsorption. Therefore, the stronger ion accumulation on the OLC/CNT-based electrode, originating from the larger curvature, leads to a larger capacitance normalized to the electrode surface area.[56,60,62] This behavior of the capacitance increasing with curvature could help enhance the supercapacitor capacitance by featuring the electrode with nanoscaled spherical and/or cylindrical curvatures. For instance, on the basis of MD simulations, Vatamanu et al.[63,64] showed that the capacitance of EDLs is increased, using electrodes with rough surfaces that exhibit similar behaviors as the nanoscaled curved electrode.

Benefitting from the excellent thermal stability of RTILs, RTIL-based supercapacitors can work under a quite wide temperature range, which broadens the application of supercapacitors under severe conditions.[65−67] A number of groups have explored the temperature influence on the capacitive behavior of supercapacitors with RTIL electrolytes. Theoretical and experimental work revealed a positive temperature dependence of capacitance (i.e., the capacitance increases with temperature),[68,69] a negative temperature dependence,[52,70] and even a complex (e.g., bell-shaped) capacitance−temperature relationship.[71] Recently, Lin et al.[65] reported that OLC-based supercapacitors with RTIL electrolytes exhibited a positive temperature-dependent capacitance, while the capacitance was almost independent of the temperature for supercapacitors with vertically aligned CNT electrodes. To gain molecular insights into the temperature dependence of capacitance, an in-depth investigation is needed by means of simulations that provide details on the atomistic level.

MD simulations were performed to model RTIL-based supercapacitors with OLC/CNT electrodes as a function of temperature.[62,67] Figure 8a shows how the capacitance changes

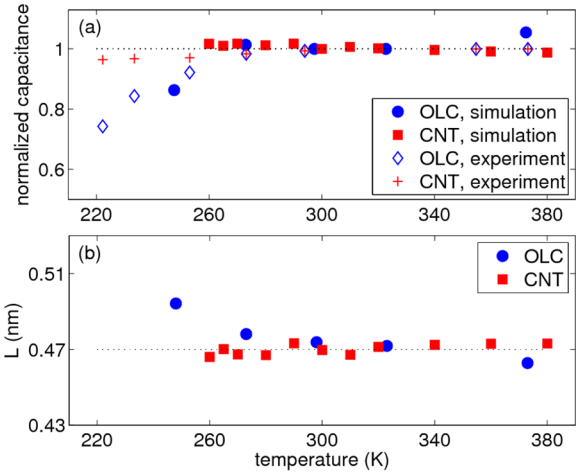

Figure 8. The temperature influence on (a) the capacitance of EDLs and (b) the effective location of counterions exohedrally near the electrode composed of OLCs with a radius of 1.22 nm or CNT with a radius of 0.41 nm. In panel a, the capacitance was normalized by that at 298 K for OLCs and by that at 300 K for CNTs; the hollow diamond and cross markers represent the experimental data from ref 65.

with temperature. It is observed that the capacitance of the OLC supercapacitor increases with temperature, whereas CNT-based supercapacitors show weak dependence of capacitance on temperature, both of which are in good agreement with the experimental observations.[65] Meanwhile, at each temperature, the differential capacitance was found to change slightly with the variation of voltage.[62,67] To understand the temperature influence on the capacitance, a MC study expatiated that a change in ion packing, in particular, the location of the counterions on the charged surface, plays a big role in the temperature dependency of the double-layer capacitance near a charged pore wall.[72] In the present work, the effective location of the counterions with respect to the electrode surface, L, was computed by the following formula

$$L = \frac{\int_{u_0}^{\text{counterion}} s^N (s - u_0) \rho_n(s)\, \mathrm{d}s}{\int_{u_0}^{\text{counterion}} s^N \rho_n(s)\, \mathrm{d}s} \tag{5}$$

where u_0 and N are the same as those defined in eq 2 and ρ_n is the number density of an EDL. One can see that in Figure 8b, the effective location of counterions adsorbed on the OLC electrode decreases as the temperature increases, while that of CNT electrode is highly insensitive to temperature. This observation can be further understood by examining the microstructure of EDLs near OLC/CNT electrodes; that is, as the temperature increases, more counterions moved toward the charged surface of the OLC electrode, whereas the number

dx.doi.org/10.1021/jz4014163 | J. Phys. Chem. Lett. 2013, 4, 3367−3376

density of counterions changed weakly for CNT supercapacitors, which eventually resulted in a positive temperature-dependent capacitance for OLC supercapacitor and the weak temperature influence on the capacitance of the CNT supercapacitor.[62,67]

In summary, MD simulations constitute a unique tool to provide detailed molecular insights into the capacitive behavior of RTIL-based supercapacitors with different types of carbon electrodes. The capacitance of porous supercapacitors was found to correlate closely with the specific nature of RTILs (e.g., structure of the ion, cation/anion size asymmetry), the generic features of pores (e.g., ion/pore interactions, short-ranged electrostatic interactions), and the applied potential. MD studies on exohedral supercapacitors show that the size or curvature of the spherical/cylindrical electrodes affects not only the magnitude of capacitance and the shape of $C-V$ curves but also the temperature dependency of the capacitance.

In the future, more efforts are required to fully understand the intricacies of charge storage mechanism of carbon supercapacitors based on RTILs.

In the future, more efforts are required to fully understand the intricacies of charge storage mechanism of carbon supercapacitors based on RTILs.

Note that in the literature, results obtained from simulations of porous electrodes have been restricted in comparison to experiment by the identical pore size at the cathode and anode and by the difference of the pore size distribution in simulation (monodisperse) and actual materials (polydisperse). The asymmetry for the pore size of the cathode and anode could lead to the different capacitive behavior as well as ion transport of porous supercapacitors. Compared with the idealized slit-shaped or cylindrical pores modeled in most studies, more realistic models for ions or/and electrodes are required, such as polarizable models for electrolyte/solvent molecules and the realistic 3-D structure of the electrode. Merlet et al.[73] performed MD simulations of the porous electrode using a 3-D complex structure with pore size distributions and SSAs similar to those in experiment, and the increased capacitance (in units of F/g) was found to be quantitatively consistent with experimental results; however, the oscillatory behavior of porous supercapacitors needs precise verification. Considering that real OLCs or CNTs have defects on the surface and could form pseudopores,[25,74] it is still unknown how the capacitance of the exohedral EDL as well as the overall supercapacitor capacitance will be affected by the ions in the interior of OLCs/CNTs and the pseudopore. From the point of view of simulation, it is hard to estimate the extent to which it is suitable to investigate supercapacitors with both endohedral and exohedral EDLs by superposing the results from the individual endohedral and exohedral supercapacitor.

Recently, in order for supercapacitors to be used under severe cold weather conditions (e.g., the lower limit for automotive applications is −50 °C), a RTIL mixture was adopted by mixing different neat RTILs to achieve a lower melting point than the neat RTIL.[65−67] For instance, Lin et al.[65] reported that the melting point of an equimolar eutectic mixture, composed of *N*-methyl-*N*-propylpiperidinium bis(fluorosulfonyl)imide ($PIP_{13}FSI$) and *N*-butyl-*N*-methylpyrrolidinium bis(fluorosulfonyl)imide ($PYR_{14}FSI$), was decreased to −80 °C, much lower than that of either component (6 or −18 °C). More explorations are required to examine the influence of the mixture on the capacitive behavior of the supercapacitor with different geometric electrodes. In addition, most investigations focus on the supercapacitor developed with RTILs consisting of monovalent ions. As a novel class of RTILs, the dicationic ionic liquids (DILs), such as a series of imidazolium- and pyrrolidinium-based geminal DILs with cations consisting of two identical imidazolium or pyrrolidinium rings linked together with alkyl chain, are attracting more and more attention in the EES community, owing to their versatility[75] and attractive properties.[76] However, very little work has been done on the interfacial structure and the electrochemical performance of DIL electrolytes in supercapacitors, even with simple geometric electrodes.

In addition to the development of supercapacitors with enhanced energy density, the improvement of power handling of supercapacitors (i.e., the charging/discharging process) is another important aspect for supercapacitors,[77] which is influenced largely by the electrolyte transport associated with ion diffusion. For example, through MD simulations of the RTIL 1-butyl-3-methylimidazolium hexafluorophosphate [bmim][PF_6] confined in a slit-shaped neutral/charged nanopore, Hung et al.[78,79] showed that the ion dynamics is highly heterogeneous and depends strongly on the distance of the ion from the pore wall; charged pore walls induce important reductions in the dynamics of the counterion. Compared with numerous studies on the properties of supercapacitors in equilibrated status, far fewer efforts using modeling have been made to investigate the dynamic process of charging/discharging of a supercapacitor cell, which will be another key research topic of this field in the future.

AUTHOR INFORMATION

Corresponding Author

*E-mail: peter.cummings@vanderbilt.edu.

Notes

The authors declare no competing financial interest.

Biographies

Guang Feng received his Ph.D. degree in 2010 from Clemson University. He joined Vanderbilt University and The Fluid Interface Reactions, Structures and Transport (FIRST) Energy Frontier Research Center as a postdoctoral research associate until now. His current research is focused on the capacitive electrical energy storage and the application of room-temperature ionic liquids. More information about his research is available at https://sites.google.com/site/fengguang668.

Song Li is a Ph.D. candidate at Vanderbilt University and a member of The Fluid Interface Reactions, Structures and Transport (FIRST) Energy Frontier Research Center. Her current research interests include structural organization and interfacial behaviors of room-temperature ionic liquids and their applications in supercapacitors.

Volker Presser received his Ph.D. in 2009 from the Eberhard Karls University, Tübingen, Germany. He joined Drexel University as a postdoctoral researcher in 2010 and was appointed Assistant Research Professor in 2011. Now he is the leader of the Junior Research Group "Energy Materials" at the INM − Leibniz-Institute for New Materials in Saarbrücken and Assistant Professor at the Saarland University. His research is focused on the development and application of novel

energy materials and water treatment technologies. More information about his research group is available at http://www.presser-group.com.

Peter T. Cummings received his Ph.D. degree in 1980 from University of Melbourne, Australia. He is the John R. Hall Professor of Chemical Engineering at Vanderbilt University and for 6 years (2007−2013) was the Principal Scientist of the Center for Nanophase Materials Sciences at Oak Ridge National Laboratory. His research interests include molecular-level modeling, electrical energy storage, and the development of new materials used in medicine, electronics, and a wide variety of industrial applications. More information about his research group is available at http://huggins.vuse.vanderbilt.edu/ptc.

■ ACKNOWLEDGMENTS

This work was supported as part of the Fluid Interface Reactions, Structures, and Transport (FIRST) Center, an Energy Frontier Research Center funded by the U.S. Department of Energy, Office of Science, Office of Basic Energy Sciences. We acknowledge the National Energy Research supercomputing Center, which is supported by the Office of Science of the U.S. Department of Energy under Contract No. DE-AC02-05CH11231. G.F. appreciates the Palmetto Cluster at Clemson University for providing computer time to complete most simulations performed for this work. V.P. acknowledges funding from the German Federal Ministry for Research and Education (BMBF) in support of the nanoEES^{3D} project (Award Number 03EK3013) as part of the strategic funding initiative energy storage framework. V.P. thanks Eduard Arzt (INM) for continuous support.

■ REFERENCES

(1) Dunn, B.; Kamath, H.; Tarascon, J.-M. Electrical Energy Storage for the Grid: A Battery of Choices. *Science* **2011**, *334*, 928−935.
(2) Miller, J. R. Valuing Reversible Energy Storage. *Science* **2012**, *335*, 1312−1313.
(3) Conway, B. E. *Electrochemical Supercapacitors: Scientific Fundamentals and Technological Applications*; Kluwer Academic/Plenum Publishers: New York, 1999.
(4) Simon, P.; Gogotsi, Y. Materials for Electrochemical Capacitors. *Nat. Mater.* **2008**, *7*, 845−854.
(5) Beguin, F.; Frackowiak, E. *Supercapacitors*; Wiley-VCH: Weinheim, Germany, 2013.
(6) Wang, J.; Polleux, J.; Lim, J.; Dunn, B. Pseudocapacitive Contributions to Electrochemical Energy Storage in TiO_2 (Anatase) Nanoparticles. *J. Phys. Chem. C* **2007**, *111*, 14925−14931.
(7) Brezesinski, K.; Wang, J.; Haetge, J.; Reitz, C.; Steinmueller, S. O.; Tolbert, S. H.; Smarsly, B. M.; Dunn, B.; Brezesinski, T. Pseudocapacitive Contributions to Charge Storage in Highly Ordered Mesoporous Group V Transition Metal Oxides with Iso-Oriented Layered Nanocrystalline Domains. *J. Am. Chem. Soc.* **2010**, *132*, 6982−6990.
(8) Ohno, H. *Electrochemical Aspects of Ionic Liquids*; Wiley-Interscience: New York, 2005.
(9) Kim, T. Y.; Lee, H. W.; Stoller, M.; Dreyer, D. R.; Bielawski, C. W.; Ruoff, R. S.; Suh, K. S. High-Performance Supercapacitors Based on Poly(Ionic Liquid)-Modified Graphene Electrodes. *ACS Nano* **2010**, *5*, 436−442.
(10) Liu, C.; Yu, Z.; Neff, D.; Zhamu, A.; Jang, B. Z. Graphene-Based Supercapacitor with an Ultrahigh Energy Density. *Nano Lett.* **2010**, *10*, 4863−4868.
(11) Armand, M.; Endres, F.; MacFarlane, D. R.; Ohno, H.; Scrosati, B. Ionic-Liquid Materials for the Electrochemical Challenges of the Future. *Nat. Mater.* **2009**, *8*, 621−629.
(12) Hu, L.; Pasta, M.; Mantia, F. L.; Cui, L.; Jeong, S.; Deshazer, H. D.; Choi, J. W.; Han, S. M.; Cui, Y. Stretchable, Porous, and Conductive Energy Textiles. *Nano Lett.* **2010**, *10*, 708−714.
(13) Zhang, L. L.; Zhao, X. S. Carbon-Based Materials as Supercapacitor Electrodes. *Chem. Soc. Rev.* **2009**, *38*, 2520−2531.
(14) Simon, P.; Gogotsi, Y. Capacitive Energy Storage in Nanostructured Carbon−Electrolyte Systems. *Acc. Chem. Res.* **2012**, *46*, 1094−1103.
(15) Marsh, H.; Reinoso, F. R. *Activated Carbon*; Elsevier: Boston, MA, 2006.
(16) Presser, V.; Heon, M.; Gogotsi, Y. Carbide-Derived Carbons — From Porous Networks to Nanotubes and Graphene. *Adv. Funct. Mater.* **2011**, *21*, 810−833.
(17) Asaka, K.; Mukai, K.; Sugino, T.; Kiyohara, K.; Takeuchi, I.; Terasawa, N.; Aida, T.; Futaba, D. N.; Hata, K.; Fukushima, T. Highly Conductive Sheets from Millimeter-Long Single-Walled Carbon Nanotubes and Ionic Liquids: Application to Fast-Moving, Low-Voltage Electromechanical Actuators Operable in Air. *Adv. Mater.* **2009**, *21*, 1582−1585.
(18) Frackowiak, E.; Jurewicz, K.; Delpeux, S.; Béguin, F. Nanotubular Materials for Supercapacitors. *J. Power Sources* **2001**, *97−98*, 822−825.
(19) Pech, D.; Brunet, M.; Durou, H.; Huang, P.; Mochalin, V.; Gogotsi, Y.; Taberna, P.-L.; Simon, P. Ultrahigh-Power Micrometre-Sized Supercapacitors Based on Onion-Like Carbon. *Nat. Nanotechnol.* **2010**, *5*, 651−654.
(20) McDonough, J. K.; Frolov, A. I.; Presser, V.; Niu, J.; Miller, C. H.; Ubieto, T.; Fedorov, M. V.; Gogotsi, Y. Influence of the Structure of Carbon Onions on Their Electrochemical Performance in Supercapacitor Electrodes. *Carbon* **2012**, *50*, 3298−3309.
(21) Miller, J. R.; Outlaw, R. A.; Holloway, B. C. Graphene Double-Layer Capacitor with AC Line-Filtering Performance. *Science* **2010**, *329*, 1637−1639.
(22) Geim, A. K.; Novoselov, K. S. The Rise of Graphene. *Nat. Mater.* **2007**, *6*, 183−191.
(23) Huang, J.; Sumpter, B. G.; Meunier, V. Theoretical Model for Nanoporous Carbon Supercapacitors. *Angew. Chem., Int. Ed.* **2008**, *47*, 520−524.
(24) Huang, J.; Sumpter, B. G.; Meunier, V. A Universal Model for Nanoporous Carbon Supercapacitors Applicable to Diverse Pore Regimes, Carbon Materials, and Electrolytes. *Chem.—Eur. J.* **2008**, *14*, 6614−6626.
(25) Huang, J.; Sumpter, B. G.; Meunier, V.; Yushin, G.; Portet, C.; Gogotsi, Y. Curvature Effects in Carbon Nanomaterials: Exohedral versus Endohedral Supercapacitors. *J. Mater. Res.* **2010**, *25*, 1525−1531.
(26) Frackowiak, E. Carbon Materials for Supercapacitor Application. *Phys. Chem. Chem. Phys.* **2007**, *9*, 1774−1785.
(27) Chmiola, J.; Yushin, G.; Gogotsi, Y.; Portet, C.; Simon, P.; Taberna, P. L. Anomalous Increase in Carbon at Pore Sizes Less Than 1 Nanometer. *Science* **2006**, *313*, 1760−1763.
(28) Raymundo-Piñero, E.; Kierzek, K.; Machnikowski, J.; Béguin, F. Relationship between the Nanoporous Texture of Activated Carbons and Their Capacitance Properties in Different Electrolytes. *Carbon* **2006**, *44*, 2498−2507.
(29) Lota, G.; Centeno, T. A.; Frackowiak, E.; Stoeckli, F. Improvement of the Structural and Chemical Properties of a Commercial Activated Carbon for Its Application in Electrochemical Capacitors. *Electrochim. Acta* **2008**, *53*, 2210−2216.
(30) Largeot, C.; Portet, C.; Chmiola, J.; Taberna, P.-L.; Gogotsi, Y.; Simon, P. Relation between the Ion Size and Pore Size for an Electric Double-Layer Capacitor. *J. Am. Chem. Soc.* **2008**, *130*, 2730−2731.
(31) Feng, G.; Qiao, R.; Huang, J.; Sumpter, B. G.; Meunier, V. Ion Distribution in Electrified Micropores and Its Role in the Anomalous Enhancement of Capacitance. *ACS Nano* **2010**, *4*, 2382−2390.
(32) Kondrat, S.; Kornyshev, A. A. Superionic State in Double-Layer Capacitors with Nanoporous Electrodes. *J. Phys.: Condens. Matter* **2011**, *23*, 022201.

(33) Kondrat, S.; Georgi, N.; Fedorov, M. V.; Kornyshev, A. A. A Superionic State in Nano-Porous Double-Layer Capacitors: Insights from Monte Carlo Simulations. *Phys. Chem. Chem. Phys.* **2011**, *13*, 11359−11366.
(34) Yang, L.; Fishbine, B. H.; Migliori, A.; Pratt, L. R. Molecular Simulation of Electric Double-Layer Capacitors Based on Carbon Nanotube Forests. *J. Am. Chem. Soc.* **2009**, *131*, 12373−12376.
(35) Shim, Y.; Kim, H. J. Nanoporous Carbon Supercapacitors in an Ionic Liquid: A Computer Simulation Study. *ACS Nano* **2010**, *4*, 2345−2355.
(36) Centeno, T. A.; Sereda, O.; Stoeckli, F. Capacitance in Carbon Pores of 0.7 to 15 nm: A Regular Pattern. *Phys. Chem. Chem. Phys.* **2011**, *13*, 12403−12406.
(37) Feng, G.; Cummings, P. T. Supercapacitor Capacitance Exhibits Oscillatory Behavior as a Function of Nanopore Size. *J. Phys. Chem. Lett.* **2011**, *2*, 2859−2864.
(38) Lin, R.; Huang, P.; Ségalini, J.; Largeot, C.; Taberna, P. L.; Chmiola, J.; Gogotsi, Y.; Simon, P. Solvent Effect on the Ion Adsorption from Ionic Liquid Electrolyte into Sub-Nanometer Carbon Pores. *Electrochim. Acta* **2009**, *54*, 7025−7032.
(39) Wu, P.; Huang, J.; Meunier, V.; Sumpter, B. G.; Qiao, R. Complex Capacitance Scaling in Ionic Liquids-Filled Nanopores. *ACS Nano* **2011**, *5*, 9044−9051.
(40) Jiang, D. E.; Jin, Z.; Wu, J. Oscillation of Capacitance inside Nanopores. *Nano Lett.* **2011**, *11*, 5373−5377.
(41) Jiang, D. E.; Jin, Z.; Henderson, D.; Wu, J. Solvent Effect on the Pore-Size Dependence of an Organic Electrolyte Supercapacitor. *J. Phys. Chem. Lett.* **2012**, *3*, 1727−1731.
(42) Wu, P.; Huang, J.; Meunier, V.; Sumpter, B. G.; Qiao, R. Voltage Dependent Charge Storage Modes and Capacity in Subnanometer Pores. *J. Phys. Chem. Lett.* **2012**, *3*, 1732−1737.
(43) Kondrat, S.; Perez, C. R.; Presser, V.; Gogotsi, Y.; Kornyshev, A. A. Effect of Pore Size and Its Dispersity on the Energy Storage in Nanoporous Supercapacitors. *Energy Environ. Sci.* **2012**, *5*, 6474−6479.
(44) Xing, L.; Vatamanu, J.; Borodin, O.; Bedrov, D. On the Atomistic Nature of Capacitance Enhancement Generated by Ionic Liquid Electrolyte Confined in Subnanometer Pores. *J. Phys. Chem. Lett.* **2012**, *4*, 132−140.
(45) Jiang, D. E.; Wu, J. Microscopic Insights into the Electrochemical Behavior of Nonaqueous Electrolytes in Electric Double-Layer Capacitors. *J. Phys. Chem. Lett.* **2013**, *4*, 1260−1267.
(46) Gogotsi, Y.; Simon, P. True Performance Metrics in Electrochemical Energy Storage. *Science* **2011**, *334*, 917−918.
(47) Kajdos, A.; Kvit, A.; Jones, F.; Jagiello, J.; Yushin, G. Tailoring the Pore Alignment for Rapid Ion Transport in Microporous Carbons. *J. Am. Chem. Soc.* **2010**, *132*, 3252−3253.
(48) Futaba, D. N.; Hata, K.; Yamada, T.; Hiraoka, T.; Hayamizu, Y.; Kakudate, Y.; Tanaike, O.; Hatori, H.; Yumura, M.; Iijima, S. Shape-Engineerable and Highly Densely Packed Single-Walled Carbon Nanotubes and Their Application as Super-Capacitor Electrodes. *Nat. Mater.* **2006**, *5*, 987−994.
(49) Izadi-Najafabadi, A.; Futaba, D. N.; Iijima, S.; Hata, K. Ion Diffusion and Electrochemical Capacitance in Aligned and Packed Single-Walled Carbon Nanotubes. *J. Am. Chem. Soc.* **2010**, *132*, 18017−18019.
(50) Kornyshev, A. A. Double-Layer in Ionic Liquids: Paradigm Change? *J. Phys. Chem. B* **2007**, *111*, 5545−5557.
(51) Lockett, V.; Horne, M.; Sedev, R.; Rodopoulos, T.; Ralston, J. Differential Capacitance of the Double Layer at the Electrode/Ionic Liquids Interface. *Phys. Chem. Chem. Phys.* **2010**, *12*, 12499−12512.
(52) Alam, M. T.; Islam, M. M.; Okajima, T.; Ohsaka, T. Measurements of Differential Capacitance at Mercury/Room-Temperature Ionic Liquids Interfaces. *J. Phys. Chem. C* **2007**, *111*, 18326−18333.
(53) Baldelli, S. Surface Structure at the Ionic Liquid-Electrified Metal Interface. *Acc. Chem. Res.* **2008**, *41*, 421−431.
(54) Trulsson, M.; Algotsson, J.; Forsman, J.; Woodward, C. E. Differential Capacitance of Room Temperature Ionic Liquids: The Role of Dispersion Forces. *J. Phys. Chem. Lett.* **2010**, *1*, 1191−1195.
(55) Feng, G.; Zhang, J. S.; Qiao, R. Microstructure and Capacitance of the Electrical Double Layers at the Interface of Ionic Liquids and Planar Electrodes. *J. Phys. Chem. C* **2009**, *113*, 4549−4559.
(56) Feng, G.; Jiang, D. E.; Cummings, P. T. Curvature Effect on the Capacitance of Electric Double Layers at Ionic Liquid/Onion-Like Carbon Interfaces. *J. Chem. Theory Comput.* **2012**, *8*, 1058−1063.
(57) Fedorov, M. V.; Kornyshev, A. A. Towards Understanding the Structure and Capacitance of Electrical Double Layer in Ionic Liquids. *Electrochim. Acta* **2008**, *53*, 6835−6840.
(58) Bazant, M. Z.; Storey, B. D.; Kornyshev, A. A. Double Layer in Ionic Liquids: Overscreening versus Crowding. *Phys. Rev. Lett.* **2011**, *106*, 046102.
(59) Georgi, N.; Kornyshev, A. A.; Fedorov, M. V. The Anatomy of the Double Layer and Capacitance in Ionic Liquids with Anisotropic Ions: Electrostriction vs. Lattice Saturation. *J. Electroanal. Chem.* **2010**, *649*, 261−267.
(60) Feng, G.; Qiao, R.; Huang, J.; Dai, S.; Sumpter, B. G.; Meunier, V. The Importance of Ion Size and Electrode Curvature on Electrical Double Layers in Ionic Liquids. *Phys. Chem. Chem. Phys.* **2011**, *13*, 1152−1161.
(61) Feng, G.; Huang, J.; Sumpter, B. G.; Meunier, V.; Qiao, R. A "Counter-Charge Layer in Generalized Solvents" Framework for Electrical Double Layers in Neat and Hybrid Ionic Liquid Electrolytes. *Phys. Chem. Chem. Phys.* **2011**, *13*, 14723−14734.
(62) Feng, G.; Li, S.; Atchison, J. S.; Presser, V.; Cummings, P. T. Molecular Insights into Carbon Nanotube Supercapacitors: Capacitance Independent of Voltage and Temperature. *J. Phys. Chem. C* **2013**, *117*, 9178−9186.
(63) Vatamanu, J.; Cao, L.; Borodin, O.; Bedrov, D.; Smith, G. D. On the Influence of Surface Topography on the Electric Double Layer Structure and Differential Capacitance of Graphite/Ionic Liquid Interfaces. *J. Phys. Chem. Lett.* **2011**, *2*, 2267−2272.
(64) Vatamanu, J.; Borodin, O.; Bedrov, D.; Smith, G. D. Molecular Dynamics Simulation Study of the Interfacial Structure and Differential Capacitance of Alkylimidazolium Bis(trifluoromethanesulfonyl)-imide [$C_n$mim][TFSI] Ionic Liquids at Graphite Electrodes. *J. Phys. Chem. C* **2012**, *116*, 7940−7951.
(65) Lin, R.; Taberna, P.-L.; Fantini, S. b.; Presser, V.; Pérez, C. R.; Malbosc, F. o.; Rupesinghe, N. L.; Teo, K. B. K.; Gogotsi, Y.; Simon, P. Capacitive Energy Storage from −50 to 100 °C Using an Ionic Liquid Electrolyte. *J. Phys. Chem. Lett.* **2011**, *2*, 2396−2401.
(66) Tsai, W.-Y.; Lin, R.; Murali, S.; Li Zhang, L.; McDonough, J. K.; Ruoff, R. S.; Taberna, P.-L.; Gogotsi, Y.; Simon, P. Outstanding Performance of Activated Graphene Based Supercapacitors in Ionic Liquid Electrolyte from −50 to 80 °C. *Nano Energy* **2013**, *2*, 403−411.
(67) Li, S.; Feng, G.; Fulvio, P. F.; Hillesheim, P. C.; Liao, C.; Dai, S.; Cummings, P. T. Molecular Dynamics Simulation Study of the Capacitive Performance of a Binary Mixture of Ionic Liquids near an Onion-Like Carbon Electrode. *J. Phys. Chem. Lett.* **2012**, *3*, 2465−2469.
(68) Lockett, V.; Sedev, R.; Ralston, J.; Horne, M.; Rodopoulos, T. Differential Capacitance of the Electrical Double Layer in Imidazolium-Based Ionic Liquids: Influence of Potential, Cation Size, and Temperature. *J. Phys. Chem. C* **2008**, *112*, 7486−7495.
(69) Silva, F.; Gomes, C.; Figueiredo, M.; Costa, R.; Martins, A.; Pereira, C. M. The Electrical Double Layer at the [BMIM][PF6] Ionic Liquid/Electrode Interface — Effect of Temperature on the Differential Capacitance. *J. Electroanal. Chem.* **2008**, *622*, 153−160.
(70) Vatamanu, J.; Borodin, O.; Smith, G. D. Molecular Insights into the Potential and Temperature Dependences of the Differential Capacitance of a Room-Temperature Ionic Liquid at Graphite Electrodes. *J. Am. Chem. Soc.* **2010**, *132*, 14825−14833.
(71) Boda, D.; Henderson, D. The Capacitance of the Solvent Primitive Model Double Layer at Low Effective Temperatures. *J. Chem. Phys.* **2000**, *112*, 8934−8938.
(72) Boda, D.; Henderson, D.; Chan, K.-Y. Monte Carlo Study of the Capacitance of the Double Layer in a Model Molten Salt. *J. Chem. Phys.* **1999**, *110*, 5346−5350.

(73) Merlet, C.; Rotenberg, B.; Madden, P. A.; Taberna, P.-L.; Simon, P.; Gogotsi, Y.; Salanne, M. On the Molecular Origin of Supercapacitance in Nanoporous Carbon Electrodes. *Nat. Mater.* **2012**, *11*, 306−310.
(74) Hantel, M. M.; Presser, V.; McDonough, J. K.; Feng, G.; Cummings, P. T.; Gogotsi, Y.; Kötz, R. In Situ Electrochemical Dilatometry of Onion-Like Carbon and Carbon Black. *J. Electrochem. Soc.* **2012**, *159*, A1897−A1903.
(75) Anderson, J. L.; Ding, R.; Ellern, A.; Armstrong, D. W. Structure and Properties of High Stability Geminal Dicationic Ionic Liquids. *J. Am. Chem. Soc.* **2004**, *127*, 593−604.
(76) Ishida, T.; Shirota, H. Dicationic Versus Monocationic Ionic Liquids: Distinctive Ionic Dynamics and Dynamical Heterogeneity. *J. Phys. Chem. B* **2012**, *117*, 1136−1150.
(77) Cagle, C.; Feng, G.; Qiao, R.; Huang, J.; Sumpter, B.; Meunier, V. Structure and Charging Kinetics of Electrical Double Layers at Large Electrode Voltages. *Microfluid. Nanofluid.* **2010**, *8*, 703−708.
(78) Singh, R.; Monk, J.; Hung, F. R. Heterogeneity in the Dynamics of the Ionic Liquid $[BMIM^+][PF_6^-]$ Confined in a Slit Nanopore. *J. Phys. Chem. C* **2011**, *115*, 16544−16554.
(79) Rajput, N. N.; Monk, J.; Hung, F. R. Structure and Dynamics of an Ionic Liquid Confined inside a Charged Slit Graphitic Nanopore. *J. Phys. Chem. C* **2012**, *116*, 14504−14513.